Eur Biophys J (2009) 38:1003–1012
DOI 10.1007/s00249-009-0497-y

ORIGINAL PAPER

Electrostatic interactions during Kv1.2 N-type inactivation: random-walk simulation

Krzysztof Małysiak · Zbigniew J. Grzywna

Received: 26 February 2009 / Revised: 17 May 2009 / Accepted: 18 May 2009 / Published online: 18 June 2009

Abstract N-type inactivation of the Kv1.2 voltage-gated potassium channel is a process in which the N-terminal of the protein (its first 20 amino acids) binds to the open-channel surface, extends and occludes its pore. This process has been experimentally studied in both intact and ShBΔ6–46 channels in which the inactivating peptides are supplied in the bath solution. In this work we provide a qualitative description of N-type inactivation by simulating the random walk of charged inactivating peptides in the electrostatic field that originates from the charges present in the channel and in the cellular membrane. Our results give a deeper insight into the previously reported influence of electrostatics on the rate of N-type inactivation of ShBΔ6–46. We also show how the enchaining of the peptides, i.e., considering the intact form of the channel, influences the N-type inactivation with different charges of those peptides.

Keywords Kv1.2 · N-type inactivation · Ball and chain · Langevin equation

Biological introduction

Kv channels belong to the group of voltage-gated cation channels, along with the sodium and calcium channels (Hille 1998). They are present in most kinds of organisms, supporting cellular electrical activity. Transduction of neural impulses, contraction of muscles, and control of cell volume are only a few examples of fundamental processes for which the action of Kv channels is essential. In the course of evolution, many different classes of K^+ channels evolved, manifesting their diversity in their biophysical properties (Hille 1998). Yet, it also appears that many functional features are shared by distinct types of Kv channels.

One of these features, the voltage modulation of the channel conductance, has been described in the classical work by Hodgkin and Huxley (1952), even without any structural information about the protein of the channel. Their hypothesis about a voltage-sensitive gate equipped with only a few charges and moved by the membrane potential has found solid support with a measurement of gating current in potassium channels (Gilly and Armstrong 1980). The advent of cloning techniques provided real insight into the structure of this gating mechanism (Papazian et al. 1991), followed by crystallographic studies that provided a visualization of the underlying structural changes.

In the Shaker family of voltage-gated potassium channels, it was found that, after a channel was opened by the strong positive voltage, it fell within milliseconds into a long-lasting nonconductive state (Hoshi et al. 1990). This process, termed fast inactivation (later N-type inactivation), was found to be coupled to the activation process and to have no intrinsic transmembrane voltage dependence (Zagotta et al. 1989, 1990). It was also established that members of the Shaker family (splice variants) that differ only in cytoplasmic segments may have different N-type inactivation kinetics. Since the action of proteolytic agents at the intracellular face of the channel slowed down or completely removed the inactivation, the "ball-and-chain" model developed originally for sodium channels has been proposed to justify the experimental facts for the potassium

K. Małysiak (✉) · Z. J. Grzywna
Department of Physical Chemistry and Technology of Polymers, Faculty of Chemistry, Silesian University of Technology, Strzody 9, Gliwice, Poland
e-mail: krzysztof.malysiak@polsl.pl

channel as well (Hoshi et al. 1990). As the name implies, the ball-and-chain mechanism assumes that the inactivation is mediated by the polypeptide ball fixed to the channel protein by a flexible chain. The ball was recognized by Zagotta et al. (1990) as the 20-residue-long N-terminus of each channel subunit, while the tether was found to be made of the next 60–80 residues.

Work done by Lagnado and Aldrich (1993a, b) provided further insight into the role of electrostatic interactions of the inactivating peptide (only the "ball") added to the solution bath with ShBΔ6–46.[1] This interaction is essentially an attraction of a positively charged ball to the negatively charged docking place. Authors have also shown that the modification of peptide hydrophobicity does not much affect the rate of inactivation (in contrast to the rate of dissociation of the peptide from its binding site). A possible explanation for this phenomenon was provided in Zhou et al. (2001), where the authors proposed that the inactivation takes place in the following sequential steps: arrival at the docking place, binding, elongation of the peptide ball, and insertion of its hydrophobic region into the pore to plug the flow of ions. Since the initial steps of the process involve hydrophobicity dependence, while the elongation and plugging rely on hydrophobic properties, it is reasonable to assume in view of previous facts that the rate of inactivation should be limited by the arrival and binding.

This hypothesis finds its confirmation in Long et al. (2005), where the authors provide the crystal structure of mammalian Kv1.2 channel with a probable binding place for the inactivating ball. This place is composed of Glu^{128}, Asp^{129}, and Glu^{130}, situated on top of the T1 domain of the channel. The distance of the binding place from the channel pore fits the probable length of the elongated inactivating peptide (ball). The elongation hypothesis is confirmed in the structure of the inactivating peptide, where the first 10 hydrophobic amino acids are followed by a sequence of positively charged residues. In the inactivated channel, hydrophobic stretch becomes buried inside the protein near the entrance to the channel selectivity filter, while charged residues are responsible for long-range electrostatic interactions (Long et al. 2005). Elongation of inactivating peptide is consistent with the experimental claim that the action of one inactivating ball suffices to induce N-type inactivation, since its presence in the channel interior cuts the flow of ions by blocking access to the selectivity filter and also prevents other peptides from entering.

As discussed above, the phenomenon of N-type inactivation has quite a detailed experimental background as well as a convincing quantitative picture. Moreover it has also been the subject of some quantitative approaches and several modeling attempts (Liebovitch et al. 1992; Małysiak and Grzywna 2008; Timpe and Peller 1995), for which the common base was the assumption about the Brownian motion of the inactivating ball before it was adsorbed to the channel. In this work, we follow with the same basic concept of randomly walking inactivating peptide. Yet our goal is to incorporate into consideration the detailed structure of the electrostatic field (originating from the channel protein and from the lipid membrane), as well as the shape of the peptide-accessible surface of the channel. Resolving the structure of the electrostatic field should enable us to follow the results of experiments from Lagnado and Aldrich (1993a) for ShBΔ6–46 to provide the answer on the existence of the dominant sources of electrostatic field present in the considered system, and further to predict the behavior of intact ShB with inactivating peptides of different charges. Additionally we will also address the matter of the influence of the rate of diffusional transport of the inactivating peptides on the overall inactivation kinetics.

Architecture of the model

In this section, we provide a detailed description of the proposed model, which is based on a three-dimensional random walk in the potential electrostatic field with mixed boundary conditions. For the case of ShBΔ6–46 and the intact channel, we use basically the same framework, yet with a different number of inactivating balls available for each channel, the justification for which will be provided in detail in the next section. Likewise, for the intact channel, we treat the polypeptide chain only as a tether for the ball, neglecting its own contribution to the random walk of the ball. A consequence of this approximation is discussed below.

Electrostatics

As a template for the protein architecture, the 2r9r structure characterized with 2.4 Å resolution was downloaded from the Protein Data Bank (http://www.pdb.org) as a biological unit, containing all four subunits of the channel positioned at the correct orientation. To follow the conditions of experiment in Lagnado and Aldrich (1993a), the β subunit was removed from the protein using PyMol software. As

[1] Throughout this work we use the following convention for naming two forms of ShB (Kv1.2): *ShBΔ6–46* is the channel with removed β subunit and with excised N-terminal; it can only inactivate with peptides from the solution. *Intact ShB* is the channel with removed β subunit; its inactivation is mediated by one of the four N-terminals of the α subunit

can be seen from comparison with Kreusch et al. (1998), the presence of the β subunit does not influence the structure of T1 much, therefore the modified 2r9r should be a valid model for the Kv1.2 α subunit. Missing atoms in the modified protein structure were added with the Swiss PdbViewer (Guex and Peitsch 1997). Records of all heteroatoms (including water molecules and potassium ions) were removed from the file. Further, the pdb file was processed by the pdb2pqr service (Dolinsky et al. 2004) to assign partial charges and radii. In this procedure, we used AMBER and CHARMM force fields to test whether the final result (i.e., the potential) depends upon the chosen field. As the differences were essentially negligible, we stuck to the CHARMM force field. During all calculations, protonation states of atoms were assigned for pH = 7 by PROPKa (Li et al. 2005). The electrostatic potential was calculated with APBS software (Baker et al. 2001) under the following conditions:

- The monovalent species ionic concentration in the solution was equal to $c_{\text{salt}} = 0.15\text{M}$ [following (Lagnado and Aldrich 1993b)].
- Dielectric constants were taken to be 2 for the protein and 78 for water.
- Solvent probe radius was set to be 1.4 Å.
- Full nonlinear Poisson-Boltzmann solver was employed.
- Boundary conditions were set to focusing, i.e., the potential calculated in the pre-run step (with the Debye-Huckel boundary) was imposed on the original calculations.

For the following system, the Debye length was found to be equal to $\lambda_{\text{D}} = 7.9$ Å. As the dimensions of the molecule were 101 × 101 × 103 Å, the computational domain was set to have 210 × 210 × 210 Å and contained the entire region where the potential generated by the protein had significantly high values. Grid spacing was initially chosen to be 0.7 Å, but then was downsampled to 1 Å without visible loss of quality.

To account for the membrane interactions, only the electrostatic part of the usual implicit membrane model was taken into account. Hydrophobic interactions with the membrane (nonpolar solvation free-energy terms) were neglected, since as Lagnado and Aldrich (1993b) suggest, rate of inactivation does not depend upon the hydrophobicity of the inactivating peptide. For the effective membrane model, we therefore used an infinite plane with continuous surface charge density σ, immersed in the ionic solution characterized by the parameters given above. For this case, the Poisson–Boltzmann equation can be solved analytically, yielding the following formula for the potential (Lipowsky and Sackmann 1995):

$$\phi(z) = \frac{2k_{\text{B}}T}{e} \ln\left[\frac{1 + \beta \exp(-z/\lambda_{\text{D}})}{1 - \beta \exp(-z/\lambda_{\text{D}})}\right] \tag{1}$$

where the parameter β is the positive root of the following quadratic equation:

$$\beta^2 + \frac{2b}{\lambda_{\text{D}}}\beta - 1 = 0 \tag{2}$$

with b being the Gouy-Chapman length

$$b = \frac{2\epsilon k_{\text{B}}T}{e|\sigma|} \tag{3}$$

Membrane surface charge density σ was estimated based on the abundance of the phosphatidylserine that constitutes 10–20% of the membrane and carries a single negative charge per molecule. Assuming the common surface area for all components of the membrane to be 72 Å^2 (Lipowsky and Sackmann 1995), we can estimate the range for the surface charge density to be $\sigma \in (-0.02, -0.045)$ C/m^2 for 10 and 20% of phosphatidylserine, respectively. Following Turnheim et al. (1999), we made the reasonable assumption that $\sigma = 0.03$ C/m^2, which translates into one electron per 534 Å^2.

Membrane potential as defined by Eqs. 1–3 was discretized and added to the already calculated protein-generated potential. Based on the calculated electrostatic field, the force acting on the randomly walking balls was estimated using the definition

$$-\nabla U(\mathbf{r}) \cdot q = \mathbf{F}(\mathbf{r}) \tag{4}$$

where $U(\mathbf{r})$ stands for the potential, q is the ball's charge, and $\mathbf{F}(\mathbf{r})$ is the force acting on the ball. For our discrete case, the grad operator was replaced by the central finite difference (or by the backward or forward differences at the boundaries). Ion accessibility surface calculated by APBS for the probe of radius 8 Å was used to estimate the shape of the protein surface that marked out the excluded volume of the channel in the simulation. Definition of force in Eq. 4 implies that the inactivating peptide is treated as a point-charge particle, which might neglect the existence of image charges or the influence of the ball on the surrounding electrolyte. Yet, as will be shown in next sections, using this simplified assumption, our model is still capable of qualitatively reproducing the experimental data.

Random walk

Random-walking inactivating balls obeyed the overdamped Langevin dynamics

$$\frac{\mathrm{d}\mathbf{r}(\mathrm{t})}{\mathrm{d}t} = \frac{\nabla U(\mathbf{r})q}{m\gamma} + \sqrt{2\frac{k_{\text{B}}T}{m\gamma}}\Gamma(t) \tag{5}$$

where $\mathbf{r}$ is the position of the moving particle, $U(\mathbf{r})$ is the electrostatic potential, m is the mass of a particle, γ stands for the damping coefficient, and Γ is the delta-correlated Gaussian white noise, with zero average and variance equal to one. Knowing the diffusion coefficient D, one may estimate the damping coefficient

$$\gamma = \frac{k_B T}{mD} \tag{6}$$

The diffusion coefficient of balls was calculated using the well-known Stokes–Einstein relation

$$D = \frac{k_B T}{6\pi\eta a} \tag{7}$$

where k_B is the Boltzmann constant, T stands for temperature (298 K), and η is the water dynamic viscosity (10^{-3} Pa s). Radius a of the inactivating ball in the water solution should be approximately 8 Å (Antz and Fakler 1998). For those data, $D = 2.7 \times 10^{-6}$ cm^2/s.

Equation 5 was discretized using the second-order stochastic Rung-Kutta algorithm (Honeycutt 1992). The Gaussian delta-correlated Langevin force was generated with the Marsaglia polar method using r250 random-number generator.

The spatial domain was the hemisphere with a radius $L = 320$ Å. This particular shape was chosen due to a planned comparison with the intact channel, where the inactivating ball's movement is limited to the hemisphere by the tether and the cellular membrane.

On the surfaces of the hemisphere, membrane, and protein, a reflecting boundary was implemented. Particles willing to cross the boundary were repelled (i.e., calculated jump was added to the current position with the opposite sign), with the exception of the place on the surface of the protein where the docking of the inactivating ball occurs. Long et al. (2005) identified three negatively charged residues (Glu^{128}, Asp^{129}, Glu^{130}) that interact with the positively charged inactivating ball and constitute the probable place for binding. Due to the tetrameric nature of the channel, there are actually four symmetrically arranged docking places, situated at the height of approximately 63 Å counting from the cytoplasmic side of the channel (marked in the Fig. 1). Yet, as previously mentioned, the adsorption of only one inactivating ball suffices to induce inactivation.

Docking place

The docking places were simulated with the reactive boundary condition. Written in terms of probability density, this condition is known as the Robin boundary condition and takes the following form

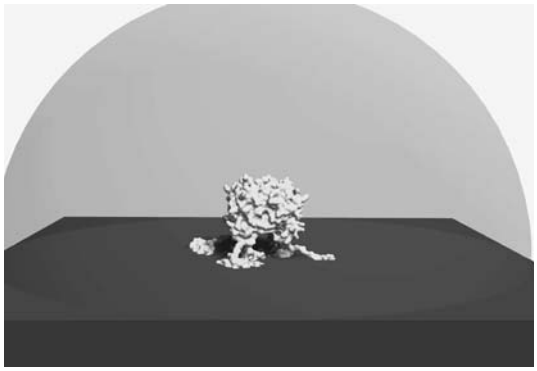

Fig. 1 Part of the hemisphere representing the spatial domain used in the simulation. Radius of the hemisphere is 320 Å, and the α subunit is buried in the membrane to the level of 55.5 Å

$$\mathbf{J}|_{AS} \cdot \mathbf{n} = -K_R \cdot c_{AS} \tag{8}$$

where c_{AS} is the concentration of the inactivating peptides in the active site, $\mathbf{n}$ is the vector perpendicular to the surface of the boundary, and $\mathbf{J}$ is the flux defined as

$$\mathbf{J}(\mathbf{r},t) = -D\nabla c(\mathbf{r},t) + \frac{-\nabla U(\mathbf{r})}{k_B T} c(\mathbf{r},t) \tag{9}$$

According to Erban and Chapman (2007), in the stochastic realization of the reactive boundary for the Langevin equation, one adsorbs the molecule that collides with this boundary with probability

$$1 - \frac{K_R\sqrt{\pi}}{2\sqrt{D}}\sqrt{\Delta t} \tag{10}$$

Even when the molecule does not touch the adsorbing boundary in the initial and final position, there is still the possibility that it happened within the Δt time. In this situation, according to Andrews and Bray (2004), the molecule is adsorbed with probability

$$\exp\left[\frac{-x(t)x(t+\Delta t)}{D\Delta t}\right]\frac{K_R\sqrt{\pi}}{2\sqrt{D}}\Delta t \tag{11}$$

Boundary condition implemented in the following way gives an opportunity to control the effectiveness of binding. By adjusting the K_R constant in Eq. 8, a reflecting ($K_R = 0$) or fully adsorbing ($K_R \to \infty$) surface results.

Estimation of the rate of inactivation

In each run of the simulation, we observed a group composed of 500–1,000 channels. Every channel was enclosed within a nonoverlapping spatial domain as shown in Fig. 2 with a properly adjusted number of inactivating peptides within. The first phase of the simulation started with the random distribution of peptides and lasted (to save computational time) until their stationary (i.e., Boltzmann)

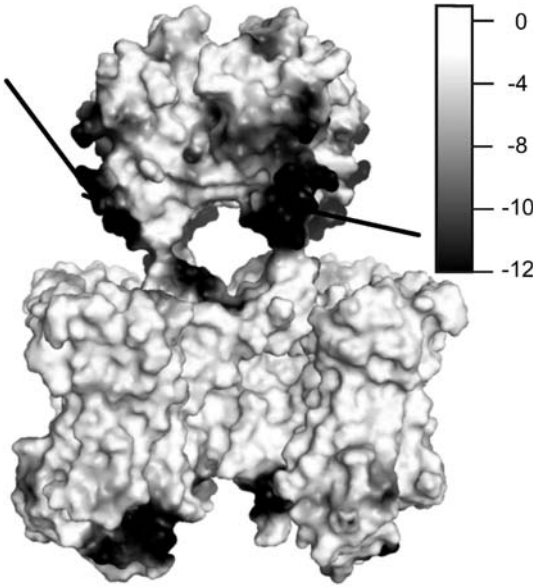

Fig. 2 Electrostatic potential calculated by APBS and mapped on the surface of the channel. *Lines* points in the direction of two visible docking sites. As might be observed, docking sites indeed show strong negative electrostatic potential. The *color bar* is scaled in millivolts

position distribution was achieved. With no possibility of binding, this reflected the open-channel situation. Then the adsorbing surface on the channel was "turned on," and the number of opened channels was measured at discrete time steps. Based on this, the survival probability SP(t) of finding a channel in the opened state was calculated. Within the registered time scales, SP(t) was found to be well approximated with a single exponential

$$\mathrm{SP}(t) \propto \exp(t/\overline{\mathrm{SP}}) \tag{12}$$

The main outcome of our simulation, the time constant $\overline{\mathrm{SP}}$ was found with nonlinear regression and is identical to the experimental time constant, since survival probability is proportional to the measured current.

Parameter estimation

Before beginning with the model, to provide a qualitative background for a given experiment, one has to carefully adjust the values of parameters that are not directly reported in the literature or cannot be directly calculated from the first principles.

Inactivating peptide concentration, ShBΔ6–46 versus intact ShB

In the experiment with excised channels, there might be more than four balls present in the channel vicinity, as from its point of view, it stays immersed in a large bath of inactivating peptides. Since we use a finite spatial domain, we have to take a proper number of balls that would mimic the contact with a solution of a known concentration. The desired number of balls is calculated in the following way. A part of the hemisphere outside the electrostatic field is chosen and considered as a bulk. For each charge of the peptide, we measure the slope of the plotted collision flux with a chosen part of the hemisphere versus the number of balls present in the system. Using slopes, we can calculate, for each charge, how many balls have to be enclosed within the hemisphere to provide the same collision flux, i.e., the same concentration in the bulk. For a particular $c_{\mathrm{bulk}} = 100\mu\mathrm{M}$ for the ball with zero charge, there are on average 3.39 balls within the hemisphere, so we can appropriately scale down the number of balls used in the simulation to keep the bulk concentration at the desired level (Table 1).

In contrast to the excised channels, where the radius of a hemisphere can be adjusted almost "on demand" (certainly a change in the hemisphere dimensions compels a change in the number of balls it contains), for the intact channels, this radius is the length of the tether, and the hemisphere always carries only four balls. Therefore in this case, the inactivation kinetics will differ with different radii, as shown experimentally by Hoshi et al. (1990).

In the course of our work, we estimated the appropriate length of the hemisphere radius for the intact channel to be 320 Å. Knowing the average distance between α carbons to be 3.8 Å (Flory 1953), this implies 80 amino acids for the tether. This value is an upper bound estimated by Zagotta et al. (1990). It might be lower, however, if one were to resolve the influence of the chain on the random walk of the ball. Having the chain included, the diffusion coefficient for the system ball + tether should be smaller than for the ball alone, which would consequently allow a shorter chain to be assumed.

Potential at the docking place

Knowing that the major portions of α-subunit helices are buried in the membrane, it is possible that the docking place will be sufficiently close to the membrane surface to stay under the influence of its electrostatic field. Therefore setting a proper distance between the membrane and the docking place should be crucial for imposing an appropriate local electrostatic potential there. Using our potential distribution calculated with APBS, we estimated an average surface potential generated by the protein at the docking place to be equal to −12 mV. Compared with the value reported by Lagnado and Aldrich (1993a), it seems that the remaining −11 mV originates from the charged surface of the membrane. Thus for the assumed membrane charge density, the distance between the membrane and the

Table 1 Number of inactivating peptides used for the case with ShBΔ6–46, together with simulation and experiment results

Charge	Slope bulk[a]	Slope docking[b]	No. of balls	Average inactivation time (s)	
				Experiment[c]	Simulation[d]
−1	4.46E+07	5.75E+04	3.14	1.17E-02	5.44E-03
0	4.12E+07	1.30E+05	3.39		2.42E-03
2	3.02E+07	6.29E+05	4.63	8.17E-04	8.52E-04
3	2.21E+07	1.18E+06	6.33		3.29E-04
4	1.39E+07	1.94E+06	10.05	2.65E-04	1.22E-04
5	7.07E+06	2.68E+06	19.78	1.08E-04	4.71E-05
6	3.40E+06	3.23E+06	41.14	2.08E-05	1.81E-05

[a] Slope of double logarithmic plot between amount of collision with a surface of the hemisphere versus ball charge

[b] Slope of double logarithmic plot between amount of collision with a docking place versus ball charge

[c] Data from Lagnado and Aldrich (1993b)

[d] Average of the exponential distribution fitted to the number of opened channels versus time

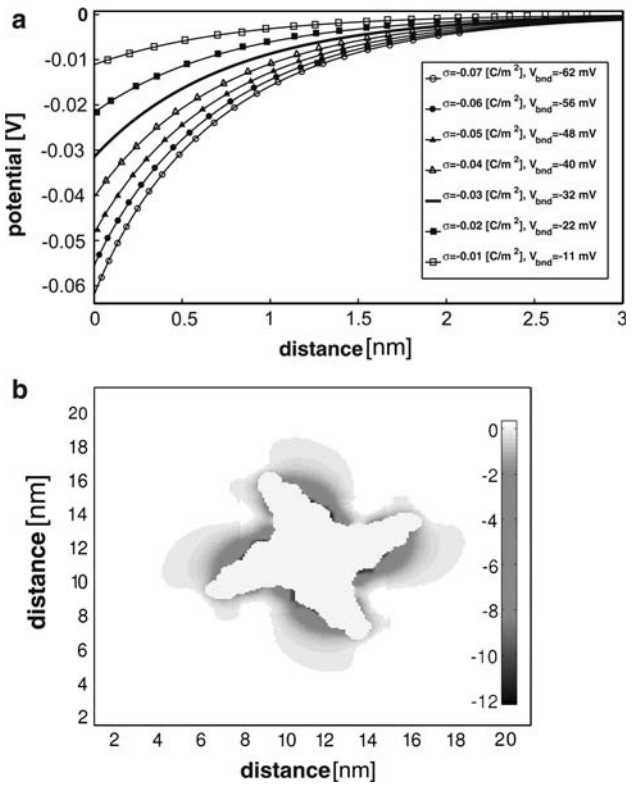

Fig. 3 **a** Electrostatic potential generated by the membrane shown along the axis perpendicular to its surface. Different curves are for the different surface charge densities. The *table* in the figure shows respective surface potentials. **b** Electrostatic potential generated by the protein shown for the plane perpendicular to the channel pore at the level of the docking sites, indicated by *arrows*. Plane is situated 8 Å above the membrane (63 Å above the extracellular site of the channel). High potentials inside the protein were overwritten to zero (spaces inaccessible for the inactivating peptide). *Color bar* is scaled in millivolts

binding site should be approximately 8 Å, as shown in Fig. 3. Assuming that the whole α-subunit is buried within the membrane, channel geometry suggests 7 Å of separation, what is close to our value obtained from the known local electrostatic potential.

Binding effectiveness

Once treated with +2 charged polypeptides of 100 μM bulk concentration, ShBΔ6–46 inactivates in an average time of 0.817 ms (cf Table 1), while the intact ShB with the same peptide inactivates within 1.6 ms (Hoshi et al. 1990). To assess the suitable binding effectiveness in our model, we performed a series of simulations with ShBΔ6–46 for different values of K_R in Eq. 8. Rate of inactivation for a given peptide charge changes linearly with K_R, which is clear from Eqs. 10 and 11.

For the fully adsorbing boundary, the average inactivation time equals 3.92×10^{-5} ms, while for $K = 2.98 \times 10^{-3}$, there is agreement with the experiment. As a consequence, and due to an overwhelming number of available peptide molecules for each channel, the effective concentration of the peptide at the docking place will be time independent and will obey the Boltzmann distribution

$$c(\mathbf{r}) = \exp\left[-\frac{U(\mathbf{r}) \cdot q \cdot e}{k_B T}\right] c_{\text{bulk}} \tag{13}$$

Using the above assumptions, one may connect the binding effectiveness with the rate constant of inactivation

$$k = K_R c_{AS} N_a A_1 \tag{14}$$

as shown in the "Appendix." Thus the dependence in Fig. 4 is justified by the following formula

$$\ln(\overline{SP}) = \ln\frac{1}{k} = \ln(K_R N_a A_1 c_{\text{bulk}})^{-1} + \frac{Ue}{k_B} Tq \tag{15}$$

As an additional test of the validity of our model and the estimation of parameters, we carried out our simulation at different ionic strengths of the electrolyte, achieved by

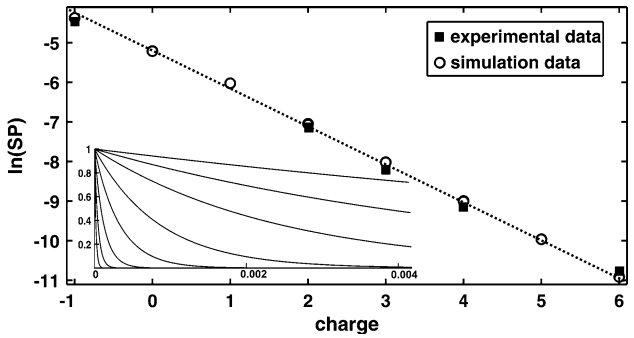

Fig. 4 Comparison of experimental and theoretical average inactivation times. *Dashed line* is just to guide the eye. Fitting results for experimental values: $y_1(x) = -0.93x - 5.41$, and for the theoretical values: $y_2(x) = -0.9071x - 5.3804$. *Nested plot* shows the decay of probability of finding a channel in the opened state as a function of time, for different charges. The *x*-axis is scaled in seconds

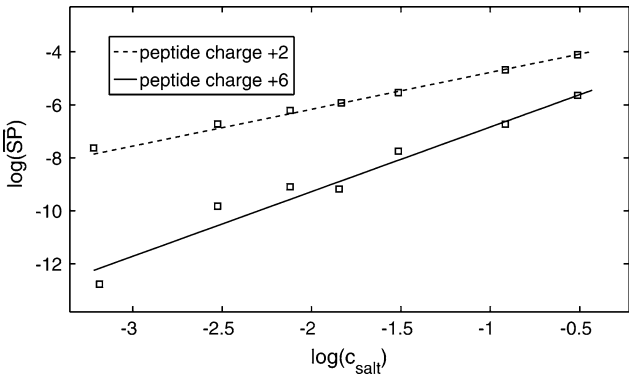

Fig. 5 Comparison of experimental and theoretical average N-type inactivation times for different inert salt concentrations. Experimental slopes are reproduced based on Lagnado and Aldrich (1993a: Fig. 1, p. 982) and are equal to $y_{+2}(x) = -1.39x - 1.47$ and $y_{+6}(x) = -5.61x - 4.4$, for +2 and +6 charges, respectively. *Squares* denote simulation results

varying the inert salt concentration c_{salt} in the electrolyte. For each salt concentration, a separate electrostatic potential map was calculated with APBS, and a separate $\varphi(z)$ was evaluated with an appropriate value of λ_D ranging from 15 to 4 Å. Comparison of simulation results with measurements from Lagnado and Aldrich (1993a) shown in Fig. 5 indicates good qualitative agreement.

Qualitative interpretation of these results is straightforward—high inert salt concentration increases the ionic strength of the solution, leading to stronger screening and weaker electrostatic attraction of the inactivating ball to the docking sites.

Intact channel

In this section, we will apply our model to examine the influence of electrostatic interactions on the intact Kv1.2

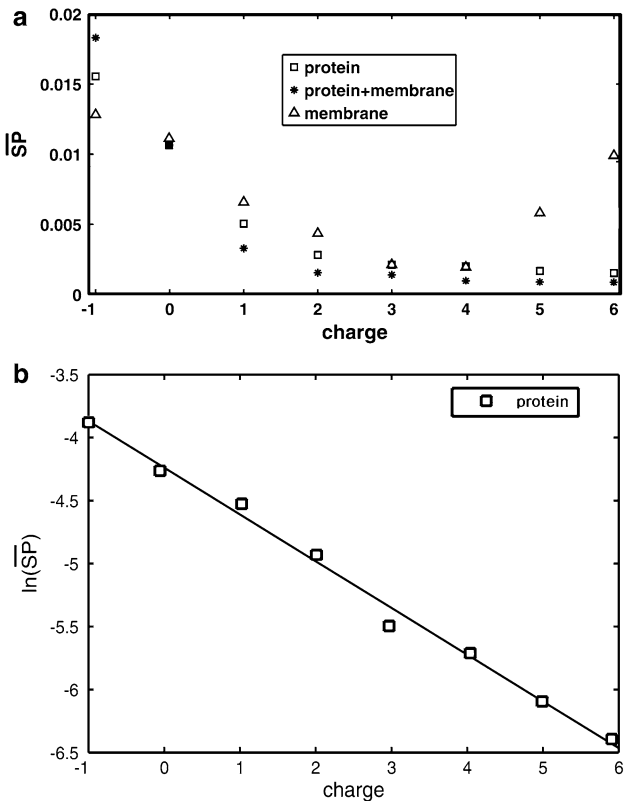

Fig. 6 **a** Average inactivation time as a function of the peptide charge for the intact channel, with selected sources of field present. For the zero-charge case, time of inactivation does not depend upon the electrostatic field. **b** For the field generated only by the protein, $\overline{\text{SP}}$ obeys Eq. 15. Fitting result is $y(x) = -0.48x - 4.24$, which converts into $U_{\text{binding}} = -12\text{mV}$

channels. All the parameters previously assigned to the model remain unchanged, excluding the number of peptides (balls and chains) present in the hemisphere, which is now fixed and equal to four. In contrast to ShBΔ6–46, for the intact channel, we no longer have a strong dependence between the inactivation rate and the peptide charge, which is shown in Fig. 6. To account for this behavior, we continued with inactivation in the separate presence of the membrane- or channel-generated potentials only.

It is clearly seen that when the protein-generated potential is the only one present in the system, then the rate of inactivation is a monotonous function of a peptide charge. Analyzing the slope, as we did previously, and using Eq. 15, one gets an average potential at the docking place equal to −12.0 mV (in agreement with the value mentioned before). This indicates that the negative potential generated by three amino acids is the strongest accessible potential for the inactivating peptide, and it dominates all the other potential wells induced by the protein.

It therefore seems that the weaker dependence of the $\overline{\text{SP}}$ may be accounted for by the membrane interactions. Change in the peptide charge from −1 to +4 results in an

increase in the local concentration of the peptides not only on the surface of the membrane, but also at the level of the binding place. Further increase in the charge leads to a further increase in the peptide concentration on the membrane surface, which results in its slower increase at the region near the binding place. This is in contrast to ShBΔ6–46, where this situation cannot occur since new peptides can arrive from the bulk, which is obviously impossible for the intact channel due to the tether. Thus, the mutual electrostatic interactions among membrane, binding site, and the inactivating peptide result in practically no difference in average inactivation times for peptide charges +5, +6. These results can be again justified by calculating the concentration profiles for the peptides that will obey the Boltzmann distribution, normalized to keep its mass (area under the curve) constant:

$$c(x,y,z) = \frac{\exp\left[-\frac{U(x,y,z)\cdot q\cdot e}{k_B T}\right]}{\int\limits_V \exp\left[-\frac{U(x,y,z)\cdot q\cdot e}{k_B T}\right] \mathrm{d}V} \frac{4N_a}{V} \tag{16}$$

where V is the volume of the available spatial region. Figure 7 illustrates the concentration distribution calculated on the basis of Eq. 16 and supports the observed behavior.

When both sources of field are present, their synergetic action shortens the time of inactivation. For higher charges, however, the action of both fields flattens the dependence, so that no substantial difference between charges +4 and +5 can be observed. For the negative peptide charge, the common interaction substantially slows the inactivation, so that in the presence of only one source, the process is faster.

Simple random-walk modeling of N-type inactivation in Liebovitch et al. (1992) has shown that

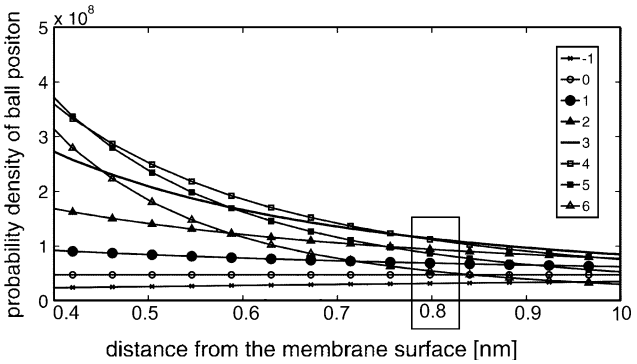

Fig. 7 Normalized concentration (stationary distribution of the peptide position) obeying the Boltzmann distribution. The *rectangle* denotes the distance from the membrane surface at which the level of concentrations resembles the order of average times of inactivation from Fig. 6. For a given order of charges: −1, 0, 6, 1, 5, 2, 4, 3, concentration of the peptides in the rectangle increases, and the corresponding rate of inactivation decreases

Table 2 Values of the exponent x defined in Eq. 17 for different peptide charges

Charge	−1	0	1	2	3	4	5	6
x	4.9	4.78	4.39	4.29	4.05	3.90	3.76	3.87

$$\overline{\mathrm{SP}} \propto L^x \tag{17}$$

where the exponent x depends upon the shape and dimensionality of the random-walk domain and upon the forces acting on the random walker. It was shown that increasing the contact of the inactivating peptide with the active site tends to decrease x, which for the system with complicated surface topology and many reflecting boundaries should take high values (Liebovitch et al. 1992). To confirm these observations, we have estimated values of x for different charges of the inactivating ball (Table 2). As might be noticed, increase in the peptide charge leads to the weaker dependence of $\overline{\mathrm{SP}}$ on the chain length L, because the attraction to the active site is stronger. Our model is characterized by a complicated geometry and force field that leads to relatively high values of x in comparison to Liebovitch et al. (1992), who indicate 3.2 for the uncharged peptide.

Conclusions

In this work we proposed a simulation of a randomly walking inactivating peptide in the potential electrostatic field, in terms of the N-type inactivation of Kv1.2 channel. The electrostatic field originated from the stationary charges present in the protein of the ion channel and from the cellular membrane. Our goal was to provide a link between the electrophysiological experiments (Lagnado and Aldrich 1993b) and physicochemical properties of the channel (in both ShBΔ6–46 and intact form) and its surroundings and to show to what extent measurements performed on one form can be used to anticipate the results for the other form. We also addressed the issue of the transport of peptides to the docking place as a rate-limiting step of inactivation.

Electrostatics

From the experimental data, it can be seen that the electrostatic interactions have a major impact on the rate of inactivation. For ShBΔ6–46, a change in a peptide charge from −1 to +6 can result in a three orders of magnitude difference in the average time of inactivation.

We have shown that by incorporating the structural details of the channel and its surroundings in our simulation, one can follow the experimental data and identify the

main factors that influence the measurement. According to our findings, it seems that for the ShBΔ6–46, the local potential at the docking place originates not only from the protein, but also from the membrane. Therefore the rate of inactivation measured from channels buried in the membranes with different surface charge densities should be substantially different. Data of this sort could provide an experimental support for our claim, yet to the best of our knowledge this issue has not been addressed experimentally.

For the intact channel, the dependence of inactivation on the peptide charge is not as strong and monotonous as for ShBΔ6–46. Presence of the charged membrane increases the rate of inactivation for small charges and decreases for large charges. As the alteration of the charge of the tethered peptide is more difficult, it seems there are no solid experimental data supporting this statement, so hopefully these findings can stimulate the research in this field.

It is worth mentioning that, for the ShBΔ6–46 case, only the local potential at the docking place determines the electrostatic dependence of inactivation, since we are dealing with an open system, and so the concentration defined by Eq. 13 does not need to conserve mass (area under the curve). In contrast to that, for the intact channel, which is a closed system, peptide concentration at a given point is influenced by all of the present charges. Thus changing the field strength far from the docking place could still have an impact on the rate of inactivation because Eq. 16 conserves the mass.

As previously mentioned however, the field generated by the docking sites dominates the protein surface, and thus especially for high charges of the inactivating peptide, one could reduce the modeling to a much simpler case, using only membrane- and docking-site-generated bistable potential. This would result in the one-dimensional random-walk process taking place in the direction perpendicular to the membrane surface with the domain bounded by the membrane and by the active site. Lower complexity of the considered system would not only decrease the computational efficiency of the simulation, but could also lead to an analytical approach using Kramers escape theory (Hänggi et al. 1990).

Nevertheless, the charge dependence of ShBΔ6–46 and intact channel inactivation rates are so different that one can barely relate one to the other.

Peptide binding and the rate-determining step

In our work we incorporate the binding process in a very simple manner. As it was shown, in essence it is a random adsorption/reflection of the peptides colliding with a binding place. This approach neglects all the physical aspects of the binding, which itself is surely a complicated process. In fact it is hard to connect the Robin constant K we used with a physical picture of the interactions between the docking place and the peptide. This is still a challenging problem, although the experimental approach has already been provided (Lagnado and Aldrich 1993a).

The last issue to address is to discuss the factors that determine the rate of inactivation. As mentioned in the introduction, there are already convincing arguments that the elongation of the adsorbed ball should be much faster than the rate of its adsorption. This work provides arguments supporting the claim that the rate of diffusional transport of peptides is also much faster than adsorption. As shown previously, diffusion-limited inactivation (with perfectly adsorbing docking place) is more than two orders of magnitude faster than experiment. It seems therefore that peptides willing to bind and inactivate the channel have to overcome some nonelectrostatic energy barrier or have to be found in the correct orientation or conformation.

Future prospects

This work seems to be the first simulation approach to the problem of N-type inactivation. Although our predictions agree with experiments, in the proposed methodology, we ignored some of the features of the system that might be important. This includes an influence of the chain in the intact channel, which has already been considered for the recovery from inactivation (Borys and Grzywna 2008). On the other hand, the simplified picture of N-type inactivation might also be a subject of some further studies. As previously mentioned, for high charges of inactivating peptides, a one-dimensional picture of the inactivating ball hopping between two potential wells might be considered, leading to the possible analytical treatment of the problem based on the Kramers rate theory. Furthermore, attachment of β-subunit to Kv1.2 could be also worth exploring, since it introduces new charged surfaces and its N-terminals can also induce N-type inactivation. It is also worth mentioning that our simulation framework can be easily generalized for other proteins where a similar mechanism controls their activity, as in the case of *Escherichia coli* iron transporter FepA (Ma et al. 2007).

Acknowledgments This study was supported by grant BW 437/RCH4/2008 from the Silesian University of Technology.

Appendix

Here we provide the justification for Eq. 14. As shown previously, diffusional transport of inactivating peptides to the binding place on the channel occurs on a time scale

much shorter than the time scale of inactivation. Thus the stationary distribution of balls (in our case the Boltzmann distribution) represents the effective concentration of balls during inactivation.

Having a population of N opened channels, the total binding area for the whole population is $A = N \times A_1$, where A_1 is the binding area supplied by the single channel. The total flux of inactivating peptides for the population of N opened channels is then (using Eq. 8)

$$J \cdot A = \frac{\mathrm{d}n_\mathrm{b}}{\mathrm{d}t} = -K_\mathrm{R} \cdot c_\mathrm{bnd} \cdot N_\mathrm{a} A \tag{18}$$

where n_b is the number of adsorbed peptides and N_a is Avogadro's number. Since all the channels in the population inactivate independently, under the constant concentration of peptides, the overall rate of inactivation follows the first-order kinetics and should be given by

$$\frac{\mathrm{dN}}{\mathrm{d}t} = -k \cdot N \tag{19}$$

Equating the rate of inactivation with the rate of peptide adsorption, one gets

$$k = K_\mathrm{R} c_\mathrm{bnd} \cdot N_\mathrm{a} A_1 \tag{20}$$

i.e., Eq. 14.

References

Andrews SS, Bray D (2004) Stochastic simulation of chemical reactions with spatial resolution and single molecule detail. Phys Biol 1(3-4):137–151

Antz C, Fakler B (1998) Fast inactivation of voltage-gated K^+ channels: from cartoon to structure. News Physiol Sci 13:177–182

Baker NA, Sept D, Joseph S, Holst MJ, McCammon AJ (2001) Electrostatics of nanosystems: application to microtubules and the ribosome. Proc Natl Acad Sci USA 98(18):10,037–10,041

Borys P, Grzywna Z (2008) On the role of ball and chain interactions in recovery from the inactivation of the shaker potassium channel. Cell Mol Biol Lett 13(4):526–534

Dolinsky TJ, Nielsen JE, McCammon JA, Baker NA (2004) Pdb2pqr: an automated pipeline for the setup of Poisson-Boltzmann electrostatics calculations. Nucl Acids Res 32:W665–W667

Erban R, Chapman SJ (2007) Reactive boundary conditions for stochastic simulations of reaction-diffusion processes. Phys Biol 4:16–29

Flory PJ (1953) Principles of polymer chemistry. Cornell University, Ithaca

Gilly WF, Armstrong CM (1980) Gating current and potassium channels in the giant axon of the squid. Biophys J 29(3):485–492

Guex N, Peitsch MC (1997) Swiss-Model and the Swiss-PdbViewer: an environment for comparative protein modeling. Electrophoresis 18(15):2714–2723

Hänggi P, Talkner P, Borkovec M (1990) Reaction-rate theory: fifty years after Kramers. Rev Mod Phys 62:251–342

Hille B (1998) Ion channels of excitable membranes. Sinauer, Sunderland

Hodgkin AL, Huxley AF (1952) A quantitative description of membrane current and its application to conduction and excitation in nerve. J Physiol 117(4):500–544

Honeycutt RL (1992) Stochastic Runge–Kutta algorithms. I. White noise. Phys Rev A 45(2):600–603

Hoshi T, Zagotta WN, Aldrich RW (1990) Biophysical and molecular mechanisms of Shaker potassium channel inactivation. Science 250(4980):533–538

Kreusch A, Pfaffinger PJ, Stevens CF, Choe S (1998) Crystal structure of the tetramerization domain of the shaker potassium channel. Nature 392(6679):945–948

Lagnado RM, Aldrich RW (1993a) Energetics of Shaker K^+ channels block by inactivation peptides. J Gen Physiol 102(6):977–1003

Lagnado RM, Aldrich RW (1993b) Interactions of amino terminal domains of Shaker K^+ channels with a pore blocking site studied with synthetic peptides. J Gen Physiol 102(6):949–975

Li H, Robertson AD, Jensen JH (2005) Very fast empirical prediction and rationalization of protein pka values. Proteins 61(4):704–721

Liebovitch LS, Selector LY, Kline RP (1992) Statistical properties predicted by the ball and chain model of channel inactivation. Biophys J 63(6):1579–1585

Lipowsky R, Sackmann E (eds) (1995) Structure and dynamics of membranes: from cells to vesicles: generic and specific interactions. Elsevier, Amsterdam

Long SB, Campbell EB, Mackinnon R (2005) Crystal structure of a mammalian voltage-dependent Shaker family K^+ channel. Science 309(5736):897–903

Ma L, Kaserer W, Annamalai R, Scott DC, Jin B, Jiang X, Xiao Q, Maymani H, Massis LM, Ferreira LCS, Newton SMC, Klebba PE (2007) Evidence of ball-and-chain transport of ferric enterobactin through fepa. J Biol Chem 282(1):397–406

Małysiak K, Grzywna ZJ (2008) On the possible methods for the mathematical description of the ball and chain model of ion channel inactivation. Cell Mol Biol Lett 13(4):535-552

Papazian DM, Timpe LC, Jan YN, Jan LY (1991) Alteration of voltage-dependence of shaker potassium channel by mutations in the s4 sequence. Nature 349(6307):305–310

Timpe LC, Peller L (1995) A random flight chain model for the tether of the shaker K+ channel inactivation domain. Biophys J 69(6):2415–2418

Turnheim K, Gruber J, Wachter C, Ruiz-Gutierrez V (1999) Membrane phospholipid composition affects function of potassium channels from rabbit colon epithelium. Am J Physiol Cell Physiol 277(1):C83–90

Zagotta WN, Hoshi T, Aldrich RW (1989) Gating of single Shaker potassium channels in Drosophila muscle and in Xenopus oocytes injected with Shaker mRNA. Proc Natl Acad Sci USA 86(18):7243–7247

Zagotta WN, Hoshi T, Aldrich RW (1990) Restoration of inactivation in mutants of Shaker potassium channels by a peptide derived from ShB. Science 250(4980):568–571

Zhou M, Morais-Cabral JH, Mann S, MacKinnon R (2001) Potassium channel receptor site for the inactivation gate and quaternary amine inhibitors. Nature 411(6838):657–661